3-4-2013

Computationally Designed Peptide Inhibitors against the Ubiquitin E3 Ligase SCF Fbx4

Bing Hao
University of Connecticut School of Medicine and Dentistry

Published in final edited form as:
Chembiochem. 2013 March 4; 14(4): 445–451. doi:10.1002/cbic.201200777.

Computationally Designed Peptide Inhibitors against the Ubiquitin E3 Ligase SCF^{Fbx4}

Junglim Lee[a,d], **Deanne W. Sammond**[a,d], **Zeno Fiorini**[a], **Jonel P. Saludes**[a], **Michael G. Resch**[b], **Bing Hao**[c], **Hang Yin**[*,a], and **Xuedong Liu**[a,*]

[a]Department of Chemistry and Biochemistry, 596 UCB, University of Colorado, JSCBB 3415 Colorado Avenue, Boulder, Colorado 80309-0215 (USA)

[b]National Renewable Energy Laboratory, 15013 Denver West Parkway, Golden, CO 80401 (USA)

[c]Molecular, Microbial and Structural Biology, University of Connecticut Health Center, 263 Farmington Avenue, Farmington, CT 06030 (USA)

Keywords

inhibitors; telomere repeat binding factor 1; E3 ligase; protein-protein interactions; ubiquitination

Telomerase is a reverse transcriptase that maintains telomere length.[1] Telomerase activity is suppressed in somatic cells such that telomere attrition triggers replicative senescence or apop-tosis.[2] In cancer cells, telomerase is up-regulated or reactivated, effectively making the cell immortal.[3] Previous studies have shown that telomerase activity positively correlates with unfavorable cancer prognosis.[4] Since it was discovered that activation of telomerase is a rate-limiting step in carcinogenesis, telomerase has gained much interest as a drug target. Both screening and structure-based methods have been extensively employed to identify small molecule leads that can selectively disrupt telomerase activity. Strategies commonly used to target telomerase activity include but are not limited to targeting the reverse transcriptase subunit of telomerase (BIBR1532 and nucleoside ananlogs),[5–7] inhibiting hTERT phosphorylation using inhibitors of protein kinase C,[8] targeting the RNA component of telomerase (peptide nucleic acids, antisense oligonucleotides - GRN163L),[9, 10] stabilizing G-quaduplex structures,[11] and using T-oligos that mimic the end of human telomeres to induce a DNA-damage response.[12] Nonetheless, with the exception of GRN163L that has recently entered into Phase III clinical trials, attempts at clinically targeting telomerase activity using classic small molecule derivatives have largely been unsuccessful.

An alternative strategy is to target proteins involved in telomere protection and maintenance. Telomeres are coated and maintained by a network of sequence-specific DNA-binding factors that tightly control telomerase activity, including TRF1, TRF2, tankyrases, and TIN2. In particular, TRF1 acts in *cis* at chromosome ends to repress telomere elongation by

Fax: (+1) 303-492-5894; (+1) 303-492-0439, xuedong.liu@colorado.edu; hang.yin@colorado.edu.
[d]These authors contributed equally to this work.

preventing telomerase from accessing the telomeres.[13] Increasing TRF1 levels will cause telomere shortening followed by replicative senescence or apoptosis.[14] Previous studies have shown that overexpression of TRF1 results in gradual telomere shortening,[13–15] whereas overexpression of dominant-negative mutants leads to telomere elongation in cells.[14, 16, 17]

A variety of factors contribute to telomere-bound TRF1 levels. Currently, two E3 ligases are known to mediate the ubiquitination and degradation of TRF1. The RING H2 zinc finger protein RLIM binds to a site adjacent to the myb domain of TRF1, and localizes to the nucleus upon binding with TRF1.[18] Studies have shown that overexpression of RLIM decreases the level of TRF1, and that shRNA knockdown of RLIM increases the level of TRF1 leading to telomere shortening and impaired cell growth.[18] SCF^{Fbx4}, on the other hand, binds to the TRFH domain of TRF1 via an atypical small GTPase domain and localizes to the cytoplasm upon binding with its substrate.[19] Zeng et al. showed that TRF1 has a higher binding affinity to TIN2 than to Fbx4,[19] and crystal structures indicate that the Fbx4-TRF1 binding interface overlaps with the TIN2-TRF1 interface, which may allow TIN2 to sequester TRF1 from Fbx4 *in vivo*. Studies have also shown that nucleostemin (NS) and guanine nucleotide binding protein-like 3 (GNL3L), GTP-binding proteins that shuttle between the nucleolar-nuclear compartments, bind to TRF1.[20] GNL3L has been shown to stabilize TRF1, whereas NS has been shown to enhance the degradation of TRF1.[21,22] Despite the complexity involved in TRF1 regulation, blocking TRF1 ubiquitination should theoretically lead to increased levels of TRF1, gradual shortening of telomeres, and replicative senescence or apoptosis.

Fbx4 functions as the substrate specific adaptor subunit of SCF^{Fbx4} that recognizes both TRF1 and cyclin D1 as substrates.[23] The interaction between TRF1 and Fbx4 was initially discovered from a two-hybrid screen.[24] It was later found that over-expression of Fbx4 reduces endogenous TRF1 levels and causes the telomeres to lengthen progressively.[23] Inhibition of Fbx4 by RNA interference (RNAi), on the other hand, stabilizes TRF1 and promotes telomere shortening, which ultimately impairs cell growth.[23] RNAi studies demonstrated that knockdown expression of Fbx4 results in stabilization of TRF1 (*19,24*). Furthermore, disabling the binding interaction between TRF1 and Fbx4 abrogates TRF1 ubiquitination both *in vitro* and *in vivo*.[19]

In this study, we directly targeted the E3 ligase (SCF^{Fbx4}) – substrate (TRF1) interface using computationally enhanced peptide inhibitors derived from the $TRF1_{TRFH}$-$Fbx4_G$ crystal structure. The approach was based on the hypothesis that TRF1-binding peptides optimized *in silico* will prevent ubiquitination - a critical step in regulating the levels of TRF1. TRF1 levels are controlled by sequential post translational modifications and subsequent degradation. ADP-ribosylation of TRF1 by tankyrase 1 releases TRF1 from telomeres, and ubiquitination of TRF1 is achieved through an enzymatic cascade, involving a series of cooperative protein-protein interactions.[25] In principle, each step is susceptible to specific inhibition. In particular, the specificity-conferring nature of E3 ligase-substrate interactions makes them prime candidates as targets for cancer therapy. However, only a few inhibitors that exploit E3 ligase-substrate interfaces are known up to this date - the Nutlins being the most thoroughly characterized among them. In the case of Nutlins, a crystal structure

determined by Pavletich et al. revealed a deep hydro-phobic pocket located at the interface of MDM2 and p53,[26, 27] prior to conducting the small-molecule screen. Such well-defined cavities have not been documented for RING domain E3s and their substrates, including and Fbx4 and TRF1. In recent years, peptides that disrupt protein-protein interactions are emerging as modulators of signaling pathways. For instance, both natural and unnatural peptide inhibitors that disrupt the MDM2-p53 interaction were identified.[28–30] However, it remains a challenge to use a rationally designed, short peptides that possess a high degree of conformational freedom to target protein-protein interfaces.

The 2.4 Å resolution crystal structure determined by Zeng et al. reveals the molecular basis by which Fbx4 recognizes TRF1.[19] In particular, the αD helix of $Fbx4_G$ reinforces the formation of the $TRF1_{TRFH}$-$Fbx4_G$ complex by contacting $TRF1_{TRFH}$ via extensive van der Waals interactions. This short helix packs against a slightly indented hydrophobic area that spans the surface of both molecules. Mutations made on both sides of the interface are sufficient to abolish $TRF1_{TRFH}$-$Fbx4_G$ binding *in vitro* and *in vivo*,[19] suggesting that it is possible to target the $TRF1_{TRFH}$-$Fbx4_G$ interface using peptides. London et al. examined 151 protein-protein structures as starting points for the derivation of high-affinity peptide segments that could be extracted from one binding partner, and used as inhibitors against the wild-type interaction.[31] Their results indicate that short linear segments contribute a majority of the binding energy for more than 50% of the examined protein-protein interactions. Evaluating the $TRF1_{TRFH}$-$Fbx4_G$ interface shows the short helical segment of $Fbx4_G$ comprising residues 339-348, contributes more than half of the total buried surface area at the interface (689 $Å^2$ of 1371 $Å^2$ total), and buries numerous hydrophobic residues. Hence, we believed that this segment is likely to provide a good starting point.

The short peptide does in fact act as an inhibitor of the wild-type interaction, with a moderate IC_{50} of 205.9 μM obtained from *in vitro* ubiquitination assays. Fluorescence polarization experi-ments show that the selected peptide binds to $TRF1_{TRFH}$ with a K_d of 41.8 μM (Table 1). While the initial peptide displays promising results, we sought to enhance its inhibitory potency of the $TRF1_{TRFH}$-$Fbx4_G$ interaction through rational peptide design.

A structure-based design protocol [32, 33] using Rosetta [34] was empolyed to enhance the affinity of a 9 residue linear segment (MPCFYLAHE - residues 339 to 347), that spans the length of the αD helix of $Fbx4_G$, to TRF1. Previous work found that protein-protein interactions can be reliably enhanced by increasing the buried hydrophobic surface area at the interface.[32] Two positions were identified as candidates for the introduction of larger hydrophobic residues, C341I and A345F. Solubility was a concern when isolating the segment from a larger globular protein. In addition, increasing the hydrophobicity of the extracted peptide in an effort to enhance binding affinity can lead to a further decrease in solubility. Thus, we replaced a solvent-exposed leucine residue with a lysine residue, L344K, and added two hydrophilic residues, S349 and K350, to the C-terminus of the peptide (Table 1). Finally, we sought to stabilize the short helical peptide by adding a C-terminal capping motif. We anticipated that these affinity-enhancing measures will provide a large contribution to the overall affinity of the peptide-TRF1 complex. In addition, we

generated two alanine substitution variants (Designs 2 and 3) to further assess the importance of the two key interface residues (F342 and F345).

To address the issues of peptide solubility, we performed analytical ultracentrifugation (AUC). Examination of the AUC data shows that Designs 1, 2, and 3 do not self-associate, and are monomers in solution (Figure S1). However, the data also suggests Designs 1 and 2 sample multiple conformations. To examine the biological activity of the peptide designs, we reconstituted Fbx4-dependent TRF1 ubiquitination *in vitro*. Although phosphorylation is not a prerequisite for ubiquitination [19], wild-type TRF1 was first phosphorylated using cyclinB-Cdk1 in the presence of ^{33}P-γ-ATP to allow quantitative detection. We then incubated TRF1 with recombinant ubiquitin, E1, E2 (UbcH5a), and the SCF^{Fbx4} complex. Increasing amounts of peptide inhibitors were added to the reaction mixture, and the relative effectiveness of the peptide inhibitors were determined by measuring the disruption of polyubiquitination, from which the IC_{50} values were generated. The tested peptides showed a range of inhibitory effects from none to more potent. The rationally optimized peptide inhibitor (Design 1) shows enhanced inhibitory activity, with an IC_{50} that is decreased by more than 6-fold (31.3 μM), showing robust inhibition of polyubiquitination compared to the minimally sized wild-type peptide lacking the modifications (IC_{50} = 205.9 μM). Both alanine substitution variants of the original design, Design 2 and 3, resulted in a loss of inhibitory activity compared to Design 1 as seen by the IC_{50} values (270.6 μM and 95.8 μM, respectively) obtained from the *in vitro* ubiquitination experiments. In contrast, control peptides 1 and 2 showed little or no inhibitory activity. However, the variation in Hill coefficients suggests that the mechanism of inhibition may be slightly different for each peptide design (Figure 2C). In summary, although all of the peptides derived from the αD helix of Fbx4 showed inhibition in the lower micromolar range, the inhibitory potency varied, with IC_{50} values ranging from 31.3 to 270.6 μM.

We then tested our computationally enhanced peptide inhibitor (Design 1) and their alanine substitution variants (Designs 2 and 3) via a fluorescence polarization binding assay to directly determine their binding affinities to $TRF1_{TRFH}$, and further assess the predicted binding mode. Peptides were labeled with 7-hydroxycoumarin as the fluorophore. Holding the peptide concentration at 0.1 μM, we added increasing concentrations of $TRF1_{TRFH}$ protein (up to 80 μM), measured polarization values, and generated equilibrium binding isotherms (Figure 4A). The dissociation constants (K_d) were determined to be 23.3 μM, 47.8 μM, 17.3 μM, and 41.8 μM for Design 1, Design 2, Design 3, and Wild-Type, respectively (Table 1). The increase in binding affinities for the computationally enhanced peptides with respect to wild-type was 1.8 to 2.4 fold - with the exception of Design 2, where a slight decrease in affinity was seen. The affinity enhancement for Design 3 suggests that the first phenylalanine residue of Design 1 contributes to binding. The role of the second phenylalaine residue in Design 1 is less clear. The negative controls, by contrast, could not be saturated within the same range of concentrations of $TRF1_{TRFH}$, or even exhibited nonspecific binding. The fluorescence polarization experiments show that, in general, the designed peptides have lower K_d values compared to the control peptides, which is consistent with their potency observed in the *in vitro* ubiquitination assays. These results suggest that differences in binding affinities between peptides and $TRF1_{TRFH}$ largely

account for the differences in the biological activities of the peptide inhibitors, although there are rare exceptions to this correlation.

It is important to note that the peptide (Design 1), which exhibited the lowest IC_{50} value, did not show the highest affinity for $TRF1_{TRFH}$. An increase in binding affinity does not always directly translate into more favorable biological activity. The fact that our binding data does not completely correlate with our *in vitro* ubiquination results is puzzling at first glance, but if we consider the muti-step and muti-component nature of the ubiquitination process, this discrepancy might not be surprising. The ubiquitin proteasome system contains a number of synergistic proteins that can potentially be influenced by distal binding events. Therefore, each component of the ubiquitination cascade can, in theory, be targeted by the peptide inhibitors: The inhibitors may be involoved in non-specific interactions at high micromolar concentrations, as implied by the *in vitro* ubiquitination control experiments (Figure 2B). Explicitly, the discrepancies between the IC_{50} values, obtained from the *in vitro* ubiquitination experiments where multiple proteins are present, and the K_d values, with only the target protein and inhibitor peptide present, suggest that non-specific and competing interactions are taking place with additional protein components. In addition, the fact that Design 3 results in decreased inhibition but tighter binding demonstrates that short peptides can adopt a number of conformations, which differs considerably from the behavior of a typical globular proteins. The difficulty in predicting and controlling such conformations poses additional challenges in peptide inhibitor design.

To elucidate the mechanism of binding, we examined whether mutations of residues located at the interface of $TRF1_{TRFH}$ could weaken or disrupt the peptide-$TRF1_{TRFH}$ interactions. The crystal structure determined by Zeng et al. [19] shows that Leu115 and L120 of $TRF1_{TRFH}$, located at the interface, both directly interact with the αD helix of Fbx4. In fact, these point mutations have been shown to disrupt the interaction of $TRF1_{TRFH}$ with $Fbx4_G$ in both GST-pull-down and yeast two-hybrid assays.[19] Therefore, we speculated that substituting these residues with a positively charged bulkier arginine residue via site directed mutagenesis will abrogate binding activity between the peptide inhibitor and $TRF1_{TRFH}$. The $TRF1_{TRFH}$ mutants, L115R and L120R, were expressed, purified, and similar fluorescence polarization assays were carried out. As speculated, the fluorescence polarization studies revealed that the mutations impair the interaction between $TRF1_{TRFH}$ and the peptides (Figure 3B and 3C). The combined site-directed mutagenesis and peptide-binding experiments suggest that certain hydrophobic interactions between the peptides and TRF1 are necessary for binding. The results of our assays also suggest that peptide-$TRF1_{TRFH}$ binding occurs in a non-promiscuous manner, and that the inhibitors act via a specific mechanism, in good agreement with the computational model.

The specificity of the design was further evaluated by assessing their effects on p27 ubiquitination. A recombinant assay system containing ubiquitin, E1, E2 (hCdc34), Cks1, p27 phosphorylated by cyclin E-Cdk2, and the SCF^{Skp2} complex was used. The SCF complex of this system is equivalent to SCF^{Fbx4} except for the fact that Fbx4 is switched out for Skp2, where Skp2 plays the critical role of specifically recognizing its substrate p27. Skp2 and Fbx4 which both belong to the F-box family, share very limited homology.[35] Our *in vitro* ubiquitination assays revealed that the computationally enhanced peptide inhibitor

has no effect on the ubiquitination of p27 (Figure S3). Taken together, the biochemical and biophysical data demonstrate that the computationally designed peptide inhibitors specifically disrupt the $TRF1_{TRFH}$-$Fbx4_G$ interaction.

With regards to specificity, the fact that Fbx4 recognizes both TRF1 and CyclinD1 makes TRF1 a slightly less than ideal target from a clinical standpoint. Both substrates are involved in the regulation of cell growth and proliferation. However, ubiquitination of cyclin D1 requires the presence of the adaptor αB-crystallin and phosphorylation at Thr286.[36] Ubiquitination of TRF1, on the other hand, does not require an adaptor protein, nor is phosphorylation of TRF1 necessary for its association with Fbx4. This implies that there may be some structural differences between the TRF-Fbx4 interaction and the Fbx4-αB-crystallin-cyclin D1 interaction. In addition, studies have shown that TIN2 and Fbx4 have overlapping TRF1-binding interfaces.[19] This suggests that TIN2 may block TRF1 recognition by Fbx4, thereby preventing SCF^{Fbx4} mediated ubiquitination and degradation. Recently, it has been shown that telomerase-negative cancer cells are capable of maintaining their telomeres by a mechanism known as alternative lengthening of telomeres (ALT). Evidence also suggests that TRF1 may have a role outside of telomere maintenance,[20] which may lead to further complications. These factors are likely to influence the practicality of targeting TRF1 degradation from a clinical standpoint, but the efficacy of the approach remains to be determined as was for the case of the FDA approved proteasome inhibitor bortezomib.[37] It is also important to note that, F142, located in the TRFH domain of TRF1, serves as a docking site for the FxLxP motif-containing proteins TIN2, PINX1, ATM, BLM, and DNA-PKcs, but does not play a significant role in the binding interaction between $TRF1_{TRFH}$ and Fbx4, which lacks the FxLxP motif. This mechanistic difference in binding may potentially be exploited in enhancing inhibitor specificity.

In summary, our studies have validated the feasibility of designing peptides that selectively disrupt E3 ligase-substrate interactions, in the absence of large binding pockets, by rationally targeting specific regions of interface. We have also demonstrat-ed the applicability of our *in silico* Rosetta protocol in increasing peptide-protein affinities. Such inhibitors have the potential to be used as drug precursors that can aid the mechanistic studies of disease related protein-protein interactions.

Experimental Section

Inhibitory peptide design

The backbone coordinates for sequence positions 339 to 347 (MPCFYLAHE) were isolated from F-box only protein 4 ($Fbx4_G$) in the $TRF1_{TRFH}$-$Fbx4_G$ complex (PDB code 3L82) for inhibitor peptide design 1. The helical region was extended in the C-terminal direction in an effort to stabilize the bound peptide conformation and thus limit the configurational entropy loss. The helix extension was achieved by aligning an alpha helix from the $TRF1_{TRFH}$ binding partner with the isolated $Fbx4_G$ helix. As a result, four additional positions were added to the helix, although the three C-terminal positions do not make contact with the target protein, $TRF1_{TRFH}$, in the model structure. The first four N-H groups and the last four C=O groups of an alpha helix lack intrahelical hydrogen bond partners, potentially destabilizing the helical secondary structure. N-terminal C-terminal helix-capping motifs

have been identified in both proteins and peptides, and are thought to provide a mechanism to stabilize the helical secondary structure.[38] A glycine-threonine-glycine motif was appended to the C-terminus of the inhibitor peptide designs to ideally act as a C-terminal helix cap. Sequence positions that had been buried in the globular Fbx4 structure became solvent exposed positions in the inhibitor peptides and thus theses positions were redesigned, allowing only polar or charged amino acids. Previous work had shown that increasing buried hydrophobic surface area could be an effective approach to enhance protein-protein binding affinity [32]. Thus, positions that were buried or peripheral to the interface between the inhibitor peptide and the target protein were redesigned in an effort to increase the buried hydrophobic surface area. Three positions from the precursor Fbx4 sequence were retained. The N-terminal position, P340, was not altered to conserve the phi-psi dihedral angles that may play a role in the interaction between the proline residue and the target protein TRF1. The position M339 was also retained. H346 was retained due to the hydrogen bonding with Y124 from the target protein. Sequence design and structural optimization was done with the molecular modeling program Rosetta.[34] A version of the Rosetta energy function with a dampened Lennard-Jones repulsion potential was used.[39]

Peptide synthesis

Solid-phase synthesis of peptides was carried out using Fmoc protected amino acids and Rink amide SS resin (200-400 mesh, Nova Biochem) on a CEM Liberty automated microwave peptide synthesizer (CEM Corporation). Dried resin was swelled in dichloromethane (30 min). The Fmoc group was removed using a solution of 20% piperidine in dimethylformamide (DMF). The deprotected resin was then suspended in a solution containing Fmoc-protected amino acid (5 eq.), HATU (5 eq.), DIPEA (10 eq.), and DMF (4 mL). Couplings were performed in duplicates. Deprotection and coupling were repeated until all residues were incorporated according to the peptide design. The fluorophore-labeled peptides were prepared on solid phase using 7- hydroxycoumarin-3-carboxylic acid (AnaSpec, Inc., CA) following the coupling conditions described above. The resulting peptides, with an amidated C-terminus and a free amino N-terminus were cleaved from resin and side-chain protecting groups were removed using a mixture of trifluoroacetic acid/water/1,2-ethanedithiol/triisopropylsilane (94:2.5:2.5:1 v/v) at room temperature (2h). The crude peptides were collected by precipitation with cold diethyl either (SigmaAldrich, MO). The peptides were purified using Agilent 1200 series semipreparative reverse phase high-performance liquid chromatrography system (Santa Clara, CA) with an Agilent Zorbax 300 SB-C8 column using a linear gradient buffer A (water/acetonitrile 9:1 v/v) and buffer B (acetonitrile), followed by lyophilization to dryness. The peptides were characterized using Matrix-assisted laser desorption/ionization time-of-flight mass spectrometer (MALDI-TOF) on a Voyager DE-STR Biospectrometry Workstation (PerSeptive Biosystems, CA).

Protein expression and purification

For the fluorescence polarization assays, $TRF1_{TRFH}$ (residues 58–268) fused to a Sumo protein and N terminal His_6 tag was expressed in *E. Coli*.[19] After a 6 hr induction using IPTG (0.1 mM) at 25°C, the cells were harvested by centrifugation. The harvested cell pellets were resuspended in lysis buffer (50 mM NaH_2PO_4, pH 8.0, 300 mM NaCl, 10 mM imidazole, 1 mM PMSF, 1mM DTT) and lysed by sonication. The lysates were cleared

using ultracentrifugation and the resulting supernatant was incubated with Ni-NTA agarose beads (1 hr) at 4°C. The beads were then washed with 20 mM imidazole and before eluting $TRF1_{TRFH}$ with 250 mM imidazole. The resulting $TRF1_{TRFH}$ was further purified using a HiLoad Superdex 200 column (GE Healthcare) after cleaving off the His_6-Sumo tag using the Ulp1 protease. For the *in vitro* ubiquitination assays, the TRF1 deletion mutant TRF1ΔMyb was expressed in *E. coli* and purified using the same procedure as for $TRF1_{TRFH}$, with the addition of two affinity purification steps using Mono-Q and Mono-S ion exchange columns (GE Healthcare). GST-tagged Fbx4 with two deletions (residues 1-54 and 150-170) was coexpressed with truncated Skp1[40] was also expressed in *E. coli* as a dicistronic message for 6 hrs at 25°C using IPTG (0.1 mM). The harvested cell pellets were resuspended in NETN buffer (Tris-base, pH 7.5, 150 mM NaCl, 1 mM EDTA, 0.5 % NP40, 1 mM DTT). After lysing the cells by sonication the cell debris was removed by ultraceltrifugation, and the supernatant was mixed with glutathione sepharose beads (QIAGEN) for 1 hr at 4°C before elution with glutathione (20 mM). The complex was then further purified by gel filtration chromatography using the HiLoad Superdex 200 column. E1, UbcH5a (E2), Cul1-Rbx1, and Skp1-Skp2 were expressed and purified as described.[41, 42]

Fluorescence polarization assay

Fluorescence polarization experiments were conducted on a Fluorolog-3 spectrofluorometer (Horiba Jobin Yvon, Inc). Coumarin-labeled peptides were dissolved into buffer (200 mM NaCl, 10mM DTT, 25 mM Tris pH 8.0). $TRF1_{TRFH}$ protein was titrated into 100 nM peptide solutions (up to 250 μM). An excitation wavelength of 302 nm and an emission wavelength of 448 nm were used. Spectra were measured using 7.0 nm slit widths at 25°C. Curve fitting and regression analysis performed using Sigma Plot 10.0 (SPSS Inc.). Data were fit to a quadratic single site binding equation Eq. (1), which was incorporated into Eq. (2) to account for the observed polarization:

$$[A{:}B]=\frac{([A_t]+[B_t]+K_d)-\sqrt{([A_t]+[B_t]+K_d)^2-4\cdot[A_t]\cdot[B_t]}}{2} \quad (1)$$

$$P_{obs}=\frac{(P_{\max}-P_o)\cdot[A{:}B]}{A_t}+P_o \quad (2)$$

where [A:B] is the concentration of coumarin labeled peptide and $TRF1_{TRFH}$ protein complex formed, $[A_t]$ is the total concentration of coumarin-labeled peptide, $[B_t]$ is the concentration of $TRF1_{TRFH}$ protein, P_{max} is the maximum polarization observed when all coumarin-labeled peptide is bound to $TRF1_{TRFH}$ protein, and P_{obs} is the measured polarization at a given concentration of $TRF1_{TRFH}$ protein. The obtained fitted parameters were for K_d, P_{max}, and P_o.

In vitro TRF1 ubiquitination assay

[γ-^{33}P]-labeled TRF1 proteins (4 mM) were generated by incubating the TRF1 with GST-cyclin B/Cdk1 (0.1 mM) in a buffer composed of Tris (50 mM, pH 8.0), $MgCl_2$ (10 mM),

ATP (10 mM), and [γ-^{33}P] ATP (2 μCi) for 1 hr. GST-cyclinB/Cdk1 was removed from the phosphorylated TRF1 by means of glutathione affinity chromatography. Ubiquitination assays were performed by incubating the phosphorylated TRF1 with E1 (0.5 mM), UbcH5a (E2; 5 mM), SCF^{Fbx4} complex (E3; 1 mM), ubiquitin (5 mM), methylated ubiquitin (100 mM), and 20X energy regeneration system (1 μL; 10 mM ATP, 20 mM HEPES [pH 7.4], 10 mM MgOAc, 300 mM creatine phosphate, and 0.5 mg/ml creatine phosphokinase) in a final volume of 15 ul. The reactions mixtures were incubated at 30°C for 2.5 hrs, and terminated by boiling after addition of Laemmli sample. The proteins were separated by SDS-PAGE and the resulting gels were dried prior to phosphoimaging analysis.

CD Spectroscopy

Spectra were recorded on a Chirascan™ - plus CD Spectrometer (Applied Photophysics) using a protein con-centration of 12 μM (0.1 cm path length). Protein concentrations were determined by UV absorbance at 280 nm. Sixteen scans from 195 to 260 nm were averaged. All spectra were measured at 25°C Results were recorded in millidegrees.

Analytical Ultracentrifugation

The hydrodynamic properties of peptides Design 1, Design 2 and Design 3 were analyzed by analytical ultracentrifugation using sedimentation velocity. The experiments were performed in a Beckman XL-I analytical ultracentrifuge (Beckman Coulter, CA) at 25°C. $S_{20,w}$ and the frictional ratio (f/f_0) was determined using Ultrascan III software using 2-D spectrum analysis and genetic algorithm. [43]

In vitro p27 ubiquitination assay

[γ-^{33}P]-labeled p27 proteins were generated by incubating the p27 with GST-cyclin E/Cdk2 (0.1 mM) in a buffer composed of Tris (50 mM, pH 8.0), $MgCl_2$ (10 mM), ATP (10 mM), and [γ-^{33}P] ATP (2 μCi) for 1 hr. The ubiquitination reaction was carried out by incubating the phosphorylated [γ-^{33}P]-labeled p27 with E1 (0.5 mM), Cdc34 (E2; 5 mM), SCF^{Skp2} complex (E3; 1 mM), Cks1 (1 mM), ubiquitin (5 mM), methylated ubiquitin (100 mM), and 20X energy regeneration system (1 μL) for 2 hrs at 30°C. The proteins were analyzed by SDS-PAGE and phosphoimaging.

Supplementary Material

Refer to Web version on PubMed Central for supplementary material.

Acknowledgments

We thank Prof. Dr. Ming Lei for discussions and reagents. This work was supported by a grants from the National Institutes of Health (CA107089; GM099948) to X.L. and B.H., and grants from a Stand Up to Cancer (SU2C) Innovative Research Award as well as a NSF CAREER Award (NSF0954819) to H.Y. We also acknowledge the U.S. Department of Energy Office of the Bio-mass Program (OBP) for funding the analytical ultracentrifuga-tion experiments.

References

1. Feng J, Funk WD, Wang SS, Weinrich SL, Avilion AA, Chiu CP, Adams RR, Chang E, Allsopp RC, Yu J, et al. Science. 1995; 269:1236. [PubMed: 7544491]

2. Schmitt CA. Nat. Rev. Cancer. 2003; 3:286. [PubMed: 12671667]
3. Kim NW, Piatyszek MA, Prowse KR, Harley CB, West MD, Ho PL, Coviello GM, Wright WE, Weinrich SL, Shay JW. Science. 1994; 266:2011. [PubMed: 7605428]
4. Shay JW. Cancer J. Sci. Am. 1998; (4 Suppl 1):S26. [PubMed: 9619268]
5. Murakami J, Nagai N, Shigemasa K, Ohama K. Eur. J. Cancer. 1999; 35:1027. [PubMed: 10533489]
6. Pascolo E, Wenz C, Lingner J, Hauel N, Priepke H, Kauffmann I, Garin-Chesa P, Rettig WJ, Damm K, Schnapp A. J. Biol. Chem. 2002; 277:15566. [PubMed: 11854300]
7. Strahl C, Blackburn EH. Nucleic Acids Res. 1994; 22:893. [PubMed: 8152919]
8. Chang JT, Lu YC, Chen YJ, Tseng CP, Chen YL, Fang CW, Cheng AJ. Br. J. Cancer. 2006; 94:870. [PubMed: 16508638]
9. Shammas MA, Simmons CG, Corey DR, Shmookler Reis RJ. Oncogene. 1999; 18:6191. [PubMed: 10597217]
10. Djojosubroto MW, Chin AC, Go N, Schaetzlein S, Manns MP, Gryaznov S, Harley CB, Rudolph KL. Hepatology. 2005; 42:1127. [PubMed: 16114043]
11. Read M, Harrison RJ, Romagnoli B, Tanious FA, Gowan SH, Reszka AP, Wilson WD, Kelland LR, Neidle S. Proc. Natl. Acad. Sci. USA. 2001; 98:4844. [PubMed: 11309493]
12. Rankin AM, Faller DV, Spanjaard RA. Anticancer Drugs. 2008; 19:329. [PubMed: 18454043]
13. Smogorzewska A, van Steensel B, Bianchi A, Oelmann S, Schaefer MR, Schnapp G, de Lange T. Mol. Cell Biol. 2000; 20:1659. [PubMed: 10669743]
14. van Steensel B, de Lange T. Nature. 1997; 385:740. [PubMed: 9034193]
15. Ancelin K, Brunori M, Bauwens S, Koering CE, Brun C, Ricoul M, Pommier JP, Sabatier L, Gilson E. Mol. Cell Biol. 2002; 22:3474. [PubMed: 11971978]
16. Karlseder J, Broccoli D, Dai Y, Hardy S, de Lange T. Science. 1999; 283:1321. [PubMed: 10037601]
17. Smogorzewska A, de Lange T. Embo J. 2002; 21:4338. [PubMed: 12169636]
18. Her YR, Chung IK. J. Biol. Chem. 2009; 284:8557. [PubMed: 19164295]
19. Zeng Z, Wang W, Yang Y, Chen Y, Yang X, Diehl JA, Liu X, Lei M. Dev. Cell. 18:214. [PubMed: 20159592]
20. Tsai RY. Cell Cycle. 2009; 8:2912. [PubMed: 19713769]
21. Zhu Q, Yasumoto H, Tsai RY. Mol. Cell Biol. 2006; 26:9279. [PubMed: 17000763]
22. Zhu Q, Meng L, Hsu JK, Lin T, Teishima J, Tsai RY. J. Cell Biol. 2009; 185:827. [PubMed: 19487455]
23. Lee TH, Perrem K, Harper JW, Lu KP, Zhou XZ. J. Biol. Chem. 2006; 281:759. [PubMed: 16275645]
24. Zhou XZ, Lu KP. Cell. 2001; 107:347. [PubMed: 11701125]
25. Chang W, Dynek JN, Smith S. Genes Dev. 2003; 17:1328. [PubMed: 12782650]
26. Vassilev LT, Vu BT, Graves B, Carvajal D, Podlaski F, Filipovic Z, Kong N, Kammlott U, Lukacs C, Klein C, Fotouhi N, Liu EA. Science. 2004; 303:844. [PubMed: 14704432]
27. Kussie PH, Gorina S, Marechal V, Elenbaas B, Moreau J, Levine AJ, Pavletich NP. Science. 1996; 274:948. [PubMed: 8875929]
28. Liu M, Li C, Pazgier M, Li C, Mao Y, Lv Y, Gu B, Wei G, Yuan W, Zhan C, Lu WY, Lu W. Proc. Natl. Acad. Sci. USA. 107:14321. [PubMed: 20660730]
29. Kritzer JA, Hodsdon ME, Schepartz A. J. Am. Chem. Soc. 2005; 127:4118. [PubMed: 15783163]
30. Kritzer JA, Zutshi R, Cheah M, Ran FA, Webman R, Wongjirad TM, Schepartz A. Chembiochem. 2006; 7:29. [PubMed: 16397877]
31. London N, Raveh B, Movshovitz-Attias D, Schueler-Furman O. Proteins. 78:3140. [PubMed: 20607702]
32. Sammond DW, Eletr ZM, Purbeck C, Kimple RJ, Siderovski DP, Kuhlman B. J. Mol. Biol. 2007; 371:1392. [PubMed: 17603074]
33. Fleishman SJ, Whitehead TA, Ekiert DC, Dreyfus C, Corn JE, Strauch EM, Wilson IA, Baker D. Science. 332:816. [PubMed: 21566186]

34. Rohl CA, Strauss CE, Misura KM, Baker D. Methods Enzymol. 2004; 383:66. [PubMed: 15063647]

35. Cenciarelli C, Chiaur DS, Guardavaccaro D, Parks W, Vidal M, Pagano M. Curr. Biol. 1999; 9:1177. [PubMed: 10531035]

36. Lin DI, Barbash O, Kumar KG, Weber JD, Harper JW, Klein-Szanto AJ, Rustgi A, Fuchs SY, Diehl JA. Mol. Cell. 2006; 24:355. [PubMed: 17081987]

37. Richardson PG, Barlogie B, Berenson J, Singhal S, Jagannath S, Irwin D, Rajkumar SV, Srkalovic G, Alsina M, Alexanian R, Siegel D, Orlowski RZ, Kuter D, Limentani SA, Lee S, Hideshima T, Esseltine DL, Kauffman M, Adams J, Schenkein DP, Anderson KC. N. Engl. J. Med. 2003; 348:2609. [PubMed: 12826635]

38. Aurora R, Rose GD. Protein Sci. 1998; 7:21. [PubMed: 9514257]

39. Dantas G, Corrent C, Reichow SL, Havranek JJ, Eletr ZM, Isern NG, Kuhlman B, Varani G, Merritt EA, Baker D. J. Mol. Biol. 2007; 366:1209. [PubMed: 17196978]

40. Schulman BA, Carrano AC, Jeffrey PD, Bowen Z, Kinnucan ER, Finnin MS, Elledge SJ, Harper JW, Pagano M, Pavletich NP. Nature. 2000; 408:381. [PubMed: 11099048]

41. Chen Y, Yang Y, van Overbeek M, Donigian JR, Baciu P, de Lange T, Lei M. Science. 2008; 319:1092. [PubMed: 18202258]

42. Hao B, Zheng N, Schulman BA, Wu G, Miller JJ, Pagano M, Pavletich NP. Mol. Cell. 2005; 20:9. [PubMed: 16209941]

43. Demeler, B. UltraScan - A Comprehensive Data Analysis Software Package for Analytical Ultracentrifugation Experiments. Modern Analytical Ultracentrifugation: Techniques and Methods. Harding, SE.; Rowe, AJ., editors. UK: Royal Society of Chemistry; 2005. p. 210-229.

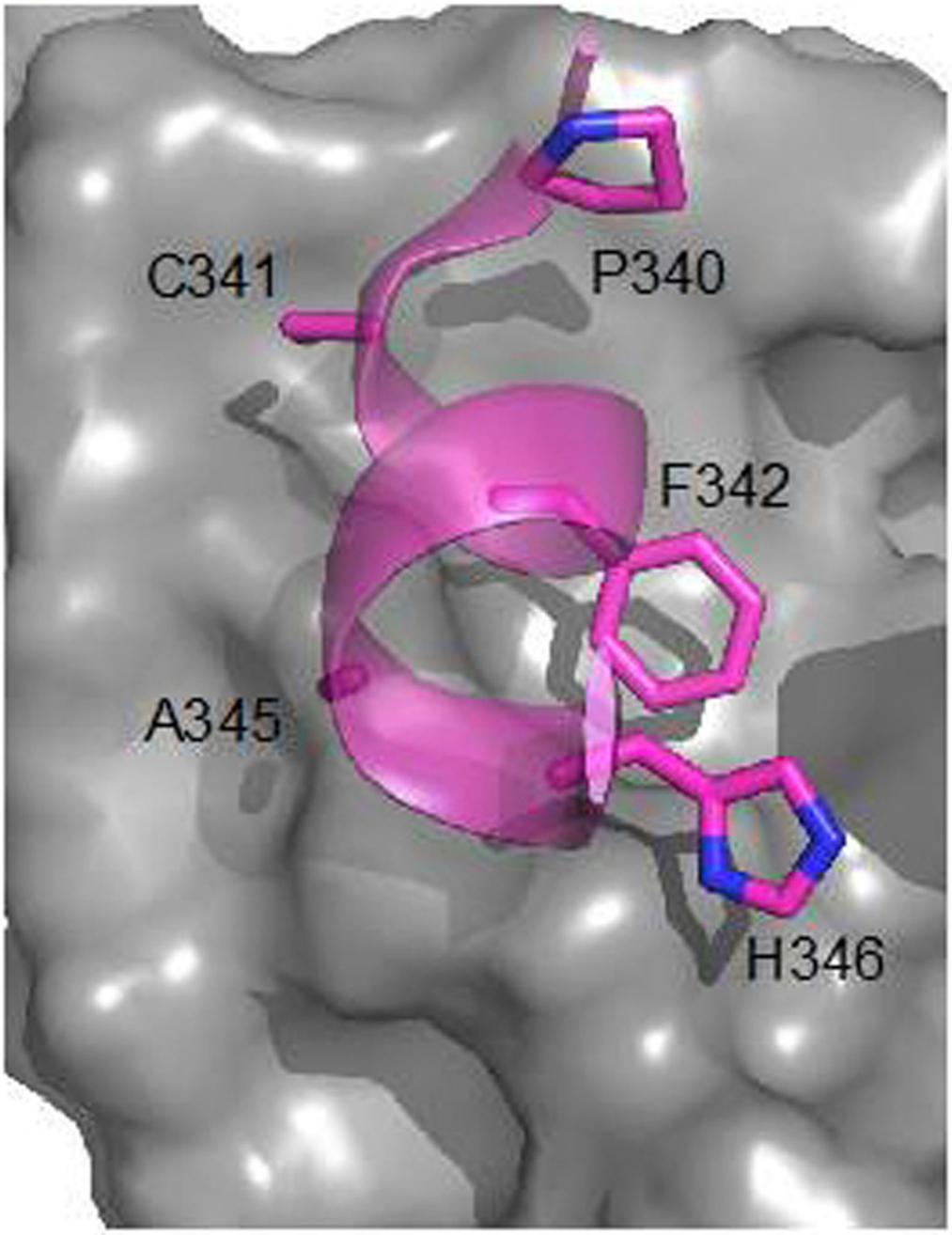

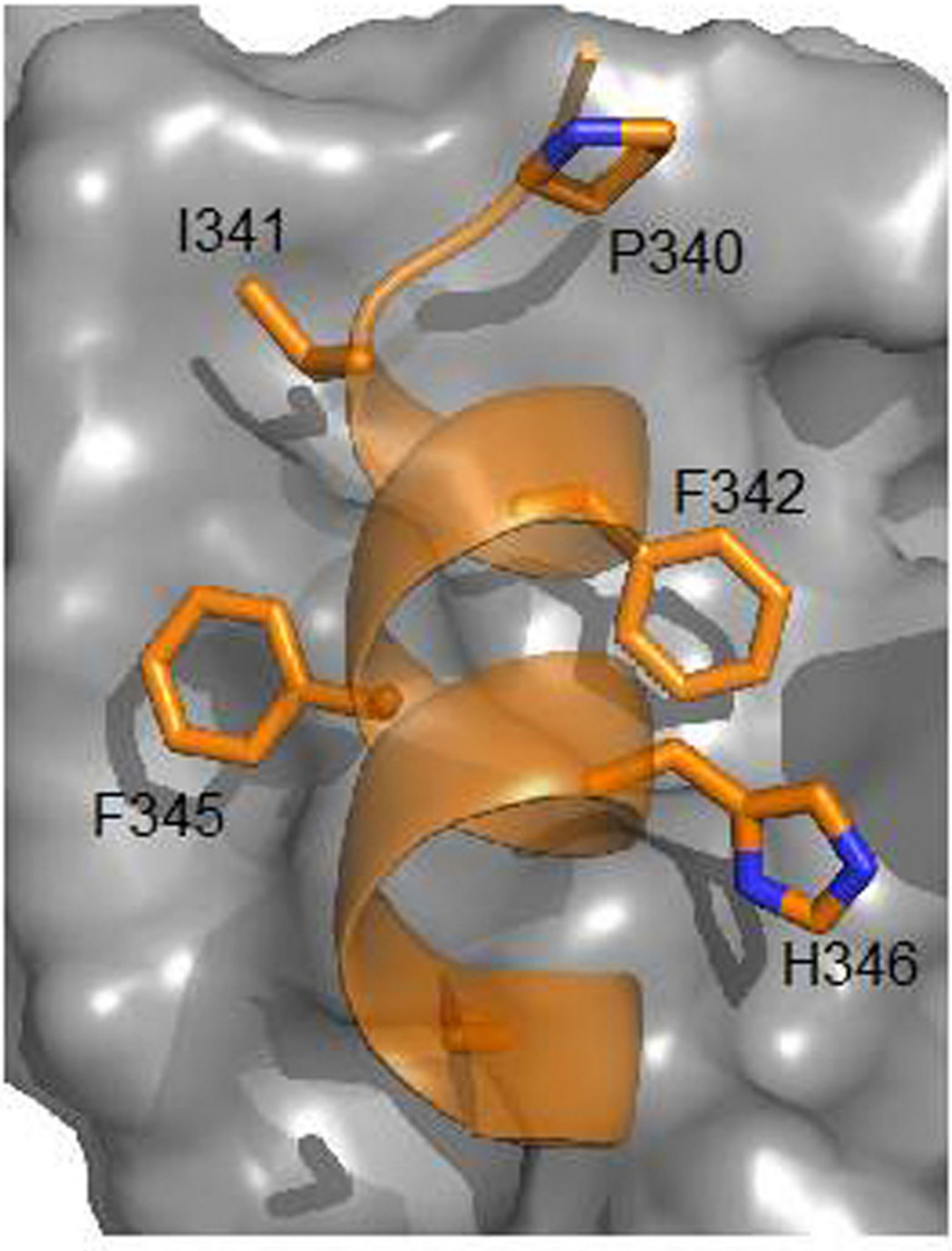

Figure 1.

Optimizing the anti-TRF1 peptide inhibitor. A) The peptide segment selected from the Fbx4 structure, shown bound to the TRF1 protein target based on the TRF1-Fbx4 crystal structure.[19] B) Model of the rationally optimized peptide inhibitor. Both the original inhibitor peptide and the rationally optimized inhibitor are shown with the same binding mode as the peptide segment (residues 339-348) cut from the FBX4 protein. The peptides are shown in cartoon representation with side chains located at key position of the interface shown and labeled. The target protein, TRF1, is shown in surface representation.

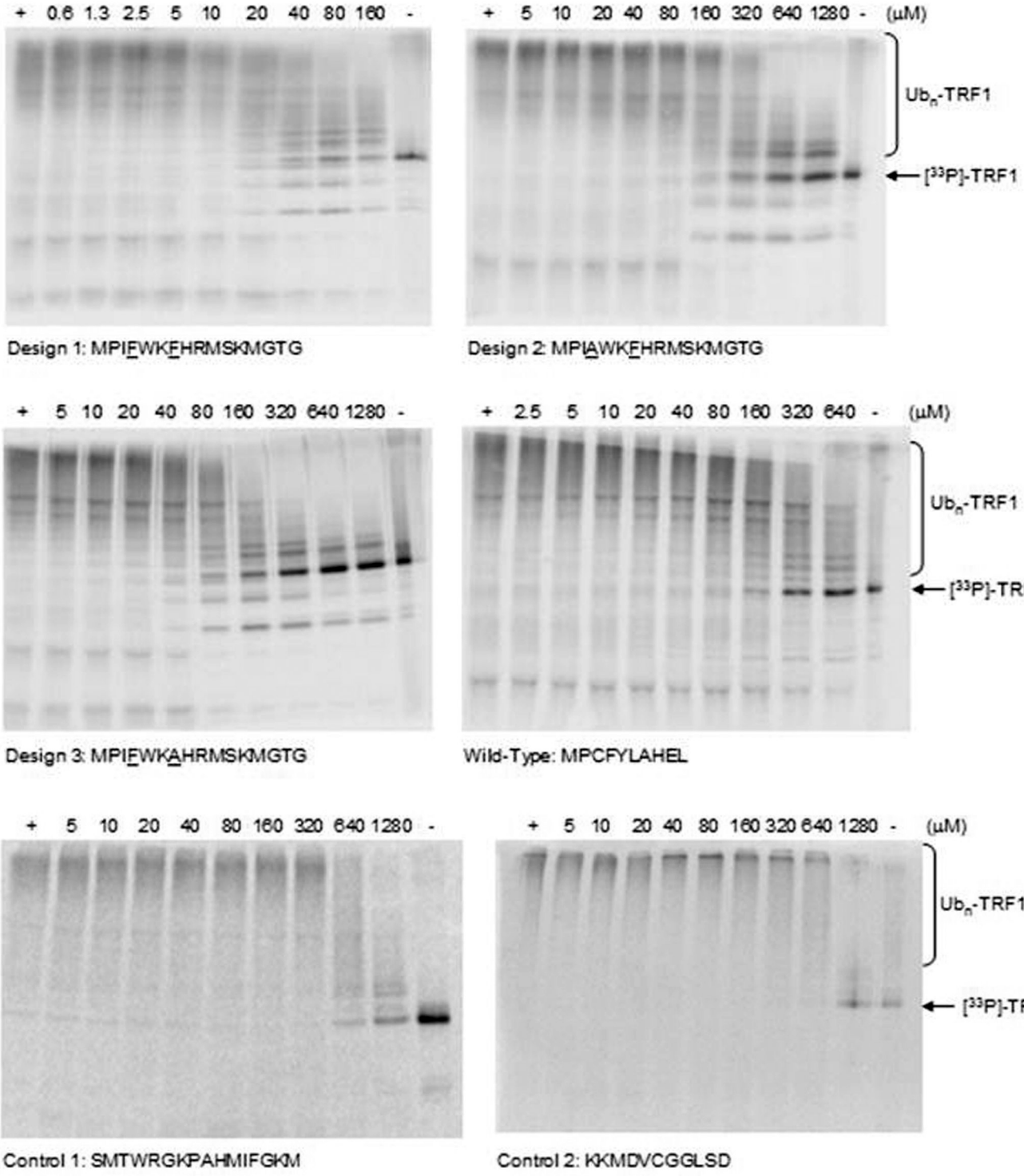

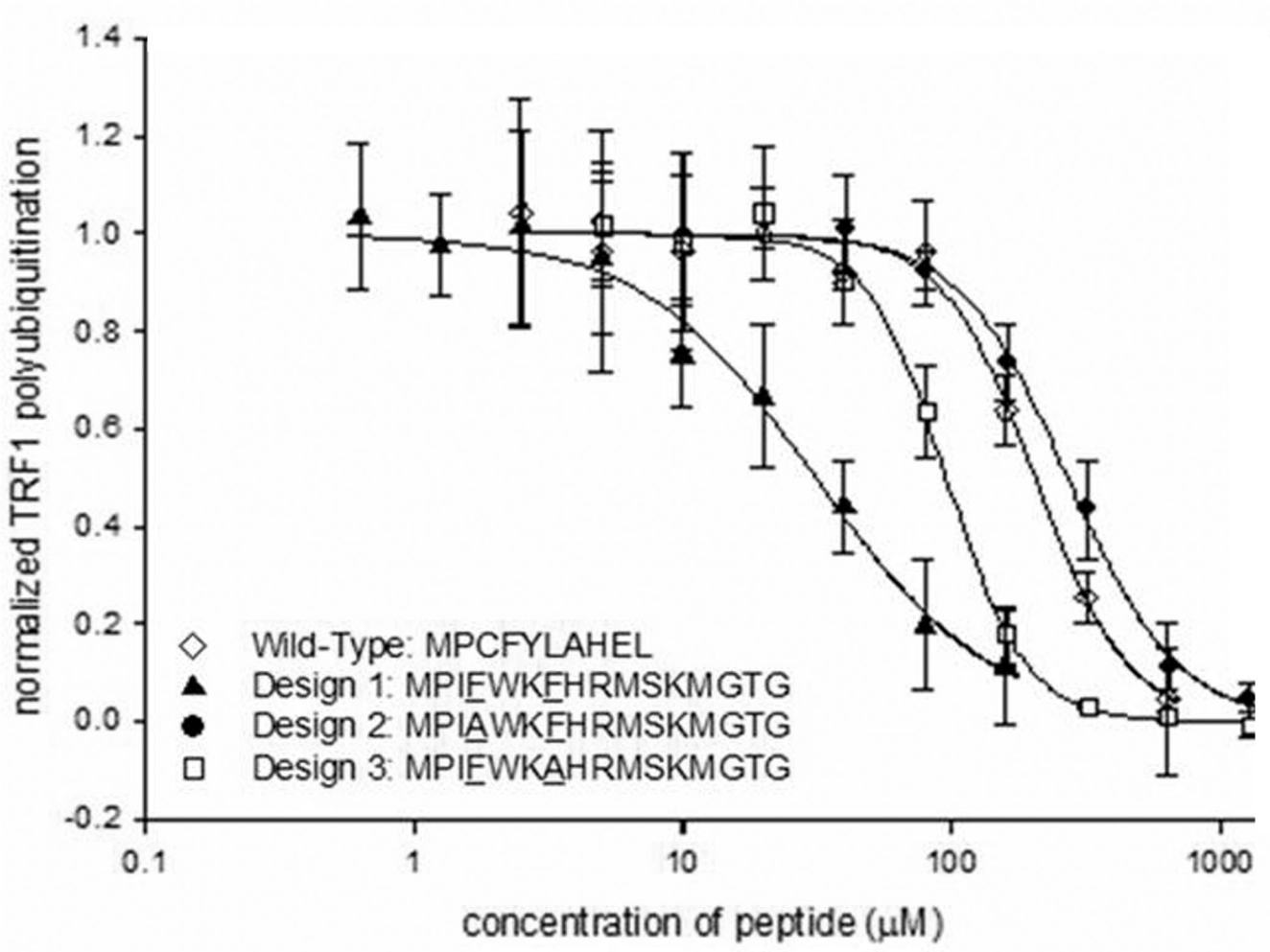

Figure 2.

Peptides inhibit polyubiquitination *in vitro*. A) Inhibition profiles of computationally enhanced peptide inhibitors. B) Inhibition profiles of control peptides. C) Normalized IC_{50} curves that represent the potency of the peptide designs. ImageJ was used to quantify the disruption of polyubiquitination. Measurements represent the mean ± standard deviation from three replicates.

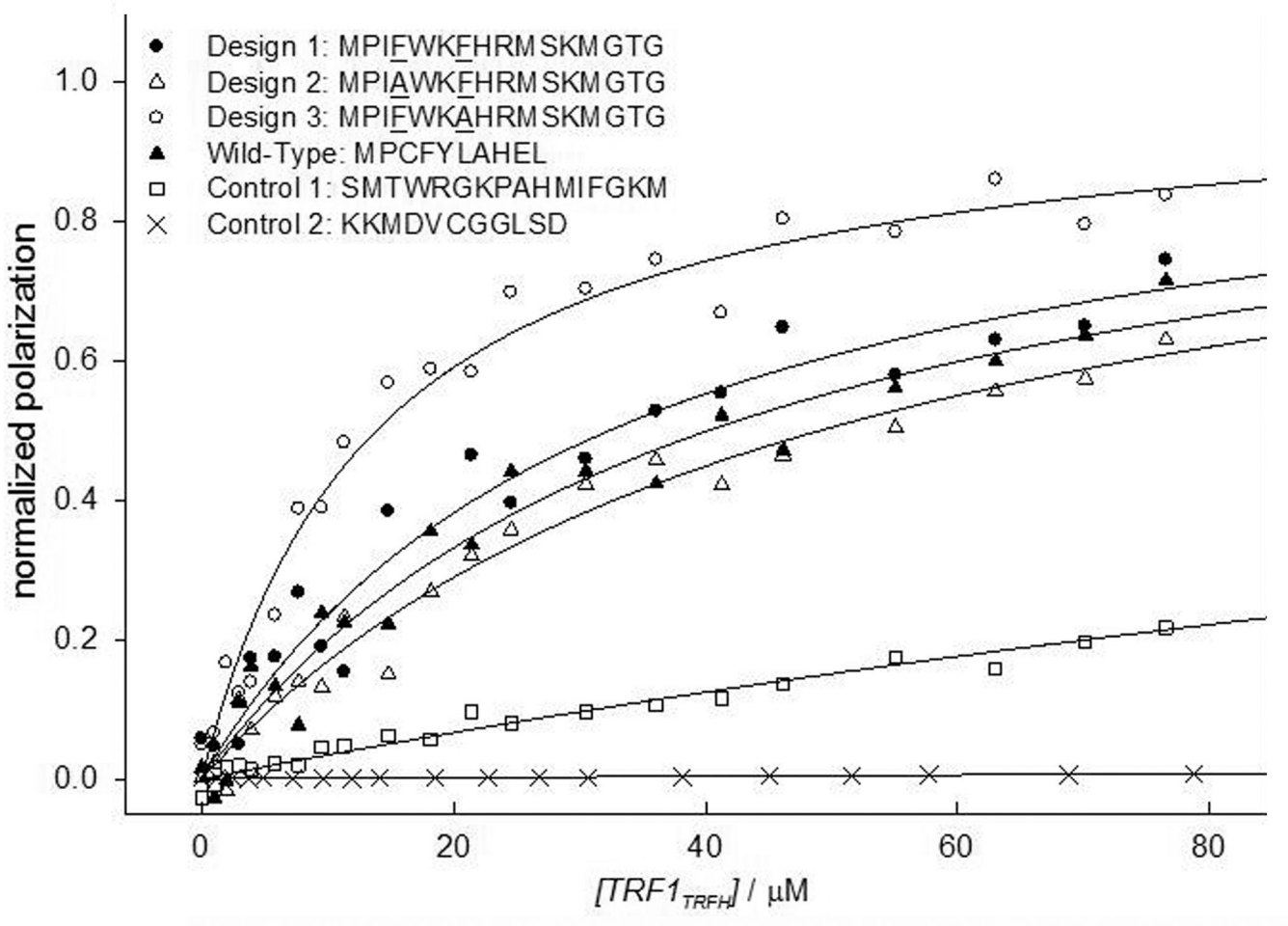

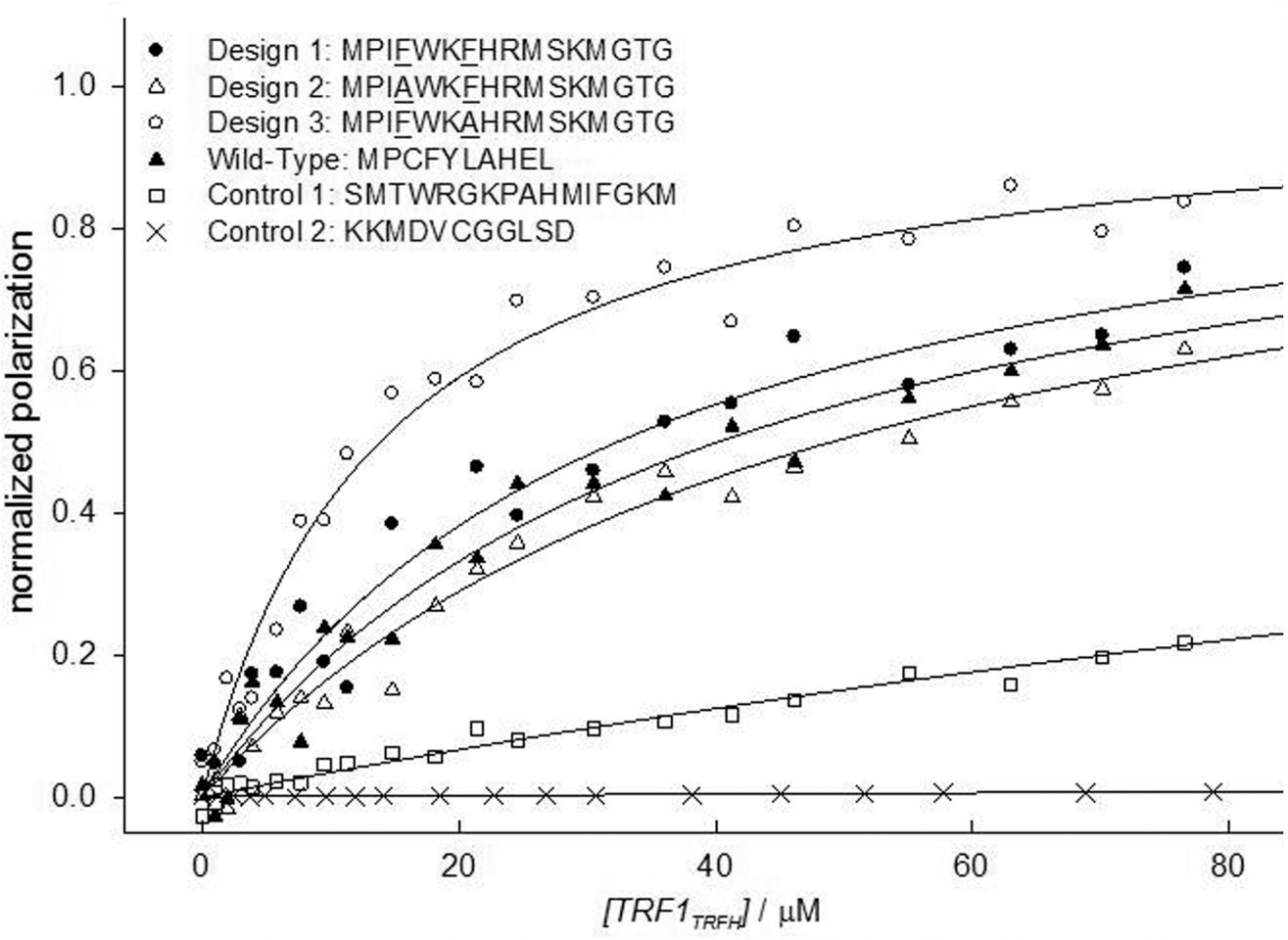

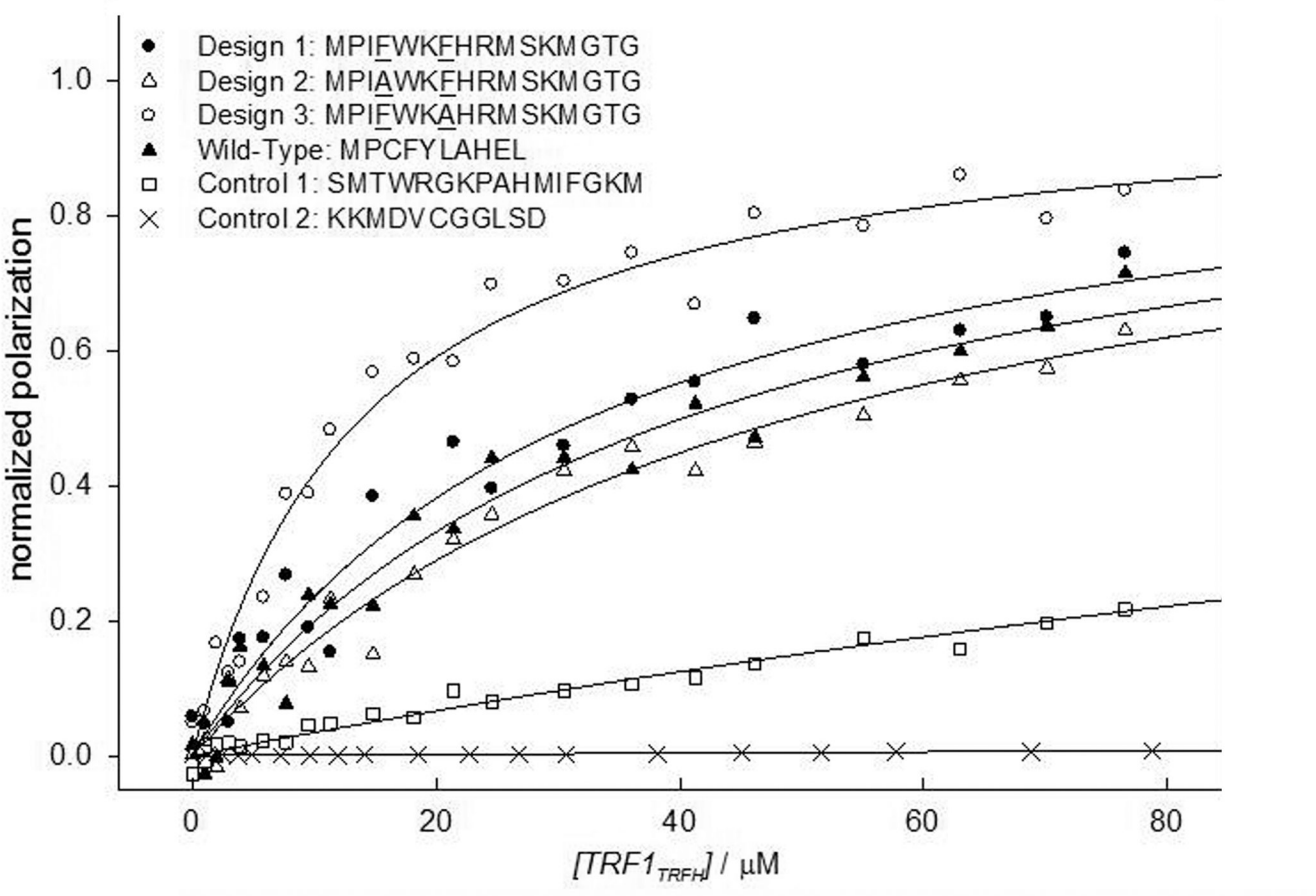

Figure 3.

WT and designed peptides bind to $TRF1_{TRFH}$, but not to $TRF1_{TRFH}^{L115R}$ or $TRF1_{TRFH}^{L120R}$. A) Fluorescence polarization confirms that the WT and designed peptides bind to TRF1TRFH. B) Mutation of Leu115 to arginine abrogates peptide protein complex formation. C) Mutation of Leu120 to arginine abrogates peptide protein complex formation.

Table 1

Experimental characterization of peptides

Peptide	Sequence	IC_{50}(μM)	K_D(μM)
Wild-Type	MPCFYLAHEL	205.9	41.8 ± 2.2
Design 1	MPIFWKFHRMSKMGTG	31.3	23.3 ± 12.8
Design 2	MPIAWKFHRMSKMGTG	270.6	47.8 ± 1.8
Design 3	MPIFWKAHRMSKMGTG	95.8	17.3 ± 4.9
Control 1	SMTWRGKPAHMIFGKM	>550	>250
Control 2	KKMDVCGGLSD	>4000	>10000

IC_{50} values were determined from the *in vitro* ubiquitination assays. Experiments were performed in triplicates. Data are expressed as mean ± standard deviation for peptide-$TRF1_{TRFH}$ complex K_D values.